the TSC genes and the *PTPN11* gene are likely to contribute to the development of ASDs in patients with these syndromes.

NF-1 is well known to be associated with ASDs. The prevalence of autism in patients with NF-1 was reported to be 4% [9]. The well-known function of the NF-1 protein is to act as a RAS-GTPase-activating protein known to be involved in the regulation of the RAS-mitogen-activated protein kinase (MAPK) pathway. Mutations in the NF-1 gene are thought to result in activation of the RAS/MAPK signal transduction pathway [2]. Clinical overlap between LEOPARD syndrome and NF-1 is also well known [19].

Approximately 50% of patients with Noonan syndrome are due to missense *PTPN11* mutations [20]. *PTPN11* encodes SHP2, a protein tyrosine phosphatase, that is involved in the activation of the RAS/MAPK cascade [2]. Noonan syndrome is caused by "gain of function" *PTPN11* mutations [1,2], and the SHP2 mutants due to the *PTPN11* mutations causing Noonan syndrome cause prolonged activation of the RAS/MAPK pathway [2]. Schubbert et al. [21] reported that germline KRAS mutations cause Noonan syndrome through the hyperactive RAS/MAPK pathway.

Herault et al. [22] reported a positive association of the HRAS gene and autism. The psychological profiles of adults and children with Noonan syndrome have been studied, and deficiencies in social and emotional recognition and expression have been identified in adults, while low verbal IQ, clumsiness, and impairment of developmental coordination have been reported in children [23].

To date, there have been no reports to suggest an association of LEOPARD syndrome and ASDs. Our observations in this familial case may suggest at least some degree of association between LEOPARD syndrome and ASD phenotypes possibly through the RAS/MAPK signal transduction pathway. Further studies with more patients with LEOPARD syndrome are needed to establish the association and to investigate the genetic contributing factors causing ASDs, leading to the prevention and earlier detection of ASDs and better management of patients with these disorders.

References

[1] Kontaridis M, Swanson KD, David FS, Barford D, Neel BG. PTPN11 (Shp2) mutations in LEOPARD syndrome have dominant negative, not activating, effects. J Biol Chem 2006;281:6785–92.

[2] Aoki Y, Niihori T, Narumi Y, Kure S, Matsubara Y. The RAS/MAPK syndromes:novel roles of the RAS pathway in human genetic disorders. Hum Mutat 2008;29:992–1006.

[3] Wing L. Autistic spectrum disorders. BMJ 1996;312:327–8.

[4] Khouzam HR, El-Gabalawi F, Pirwani N, Priest F. Asperger's disorder: a review of its diagnosis and treatment. Comp Psychiatr 2004;45:181–91.

[5] American Psychiatric Association. Diagnostic and Statistical Manual of Mental Disorders. 4th ed.-Text Revision. Washington, DC: American Psychiatric Association; 2000.

[6] Muhle R, Trentacose SV, Rapin I. The genetics of autism. Pediatrics 2004;113:e472–86.

[7] Curatolo P. Tuberous sclerosis: genes, brain, and behavior. Dev Med Child Neurol 2006;48:404.

[8] Gillberg C, Forsell C. Childhood psychosis and neurofibromatosis-More than a coincidence? J Autism Dev Disord 1984;14:1–8.

[9] Williams PG, Hersh JH. The association of neurofibromatosis Type I and autism. J Autism Dev Disord 1998;28:567–71.

[10] Cohen IL, Sudhalter V, Pfadt A, Jenkins EC, Brown WT, Vietze PM. Why are autism and the fragile-X syndrome associated? Conceptual and methodological issues. Am J Hum Genet 1991;48:195–202.

[11] Verhoeven W, Wingbermuhle E, Egger J, Van der Burgt I, Tuinier S. Noonan syndrome: psychological and psychiatric aspects. Am J Med Genet A 2008;146A:191–6.

[12] Ghaziuddin M, Bolyard B, Alessi N. Autistic disorder in Noonan syndrome. J Intell Disabil Res 1994;38:67–72.

[13] Niihori T, Aoki Y, Ohashi H, Kurosawa K, Kondoh T, Ishikiriyama S, et al. Functional analysis of PTPN11/SHP-2 mutants identified in Noonan syndrome and childhood leukemia. J Hum Genet 2005;50:192–202.

[14] Ehlers S, Gillberg C, Wing L. A screening questionnaire for Asperger syndrome and other high-functioning autism spectrum disorders in school age children. J Autism Dev Disord 1999;29:129–41.

[15] Wahlstrom J, Gillberg C, Gustavson KH, Holmgren G. A Swedish multicenter study. Am J Med Genet 1986;23:403–8.

[16] Tranebjaerg L, Kure P. Prevalence of fra (X) and other specific diagnoses in autistic individuals in a Danish county. Am J Med Genet 1991;38:212–4.

[17] Ke Y, Zhang EE, Hagihara K, Wu D, Pang Y, Klein R, et al. Deletion of Shp2 in the brain leads to defective proliferation and differentiation in neural stem cells, and early postnatal lethality. Mol Cell Biol 2007;27:6706–17.

[18] Karbowniczek M, Cash T, Cheung M, Robertson GP, Astrinidis A, Henske EP. Regulation of B-Raf kinase activity by Tuberin and Rheb is mammalian target of Rapamycin (mTOR)-independent. J Biol Chem 2004;279:29930–7.

[19] Sarkozy A, Conti E, Digilio MC, Marino B, Morini E, Pacileo G, et al. J Med Genet 2004;41:e68.

[20] Tartaglia M, Mehler EL, Goldberg R, Zampino G, Brunner HG, Kremer H, et al. Mutations in PTPN11, encoding the protein tyrosine phosphatase SHP-2, cause Noonan syndrome. Nat Genet 2001;29:465–8.

[21] Schubbert S, Zenker M, Rowe SL, Boll S, Klein C, Bollag G, et al. Germline KRAS mutations cause Noonan syndrome. Nat Genet 2006;38:331–6.

[22] Herault J, Petit E, Martineau J, Perrot A, Lenoir P, Cherpi C, et al. Autism and genetics: clinical approach and association study with two markers of HRAS gene. Am J Med Genet 1995;60:276–81.

[23] Lee DA, Portnoy S, Hill P, Gillberg C, Patton MA. Psychological profile of children with Noonan syndrome. Dev Med Child Neurol 2005;47:35–8.

Endocrine Journal 2011, **58** (3), 155-159

ORIGINAL

Identification of chromosome 15q26 terminal deletion with telomere sequences and its bearing on genotype-phenotype analysis

Sumito Dateki[1), 2)], Maki Fukami[1)], Yoko Tanaka[3)], Goro Sasaki[3)], Hiroyuki Moriuchi[2)] and Tsutomu Ogata[1)]

[1)] *Department of Molecular Endocrinology, National Research Institute for Child Health and Development, Tokyo 157-8535, Japan*
[2)] *Department of Pediatrics, Nagasaki University Graduate School of Biomedical Sciences, Nagasaki 852-8501, Japan*
[3)] *Department of Pediatrics, Tokyo Dental College Ichikawa General Hospital, Ichikawa 272-8513, Japan*

Abstract. We report a *de novo* heterozygous 5,013,940 bp terminal deletion of chromosome 15q26 in a 13 9/12 -year-old Japanese girl with short stature (–3.9 SD), mild mental retardation, and ventricular septal defect (VSD). This terminal deletion involved *IGF1R* but not *NR2F2*, and was associated with an addition of telomere repeat sequences (TTAGGG) at the end of the truncated chromosome. The results provide further support for the notion that terminal deletions are healed by *de novo* addition of telomere sequences essential for chromosome stability and DNA replication. Furthermore, while growth failure and mental retardation are primarily explained by loss of *IGF1R*, the occurrence of VSD might suggest the existence of a cardiac anomaly gene, other than the candidate cardiac anomaly gene *NR2F2*, in the deleted region.

Key words: 15q deletion, *IGF1R*, Telomere, Congenital heart defect

TERMINAL deletions of chromosome 15q are relatively rare chromosomal anomalies that are usually associated with variable degrees of pre- and post-natal growth failure and are sometimes accompanied by mental retardation and/or congenital anomalies such as congenital heart defect (CHD) [1]. In this regard, haploinsufficiency of the gene for insulin-like growth factor 1 receptor (*IGF1R*) at 15q26.3 is known to be relevant to the growth failure and mental retardation [2], and hemizygosity of the gene for nuclear receptor subfamily group F member 2 (*NR2F2*) at 15q26.2 has been postulated as an underlying factor for CHD [3–6].

The chromosome end is associated with 3–20 kb of tandemly repeated telomere sequences $(TTAGGG)_n$ that are extended and maintained in human germline by telomerase using an integral telomere-complementary RNA template [7–9]. The telomere sequences are essential for chromosome stability and DNA replication. Indeed, eukaryotic chromosomes with terminal deletions undergo end-fusion and degradation events in the absence of functional telomeres. Thus, truncated chromosomes must be healed by a *de novo* telomere addition, to replicate and segregate normally [10, 11].

Here, we report clinical and molecular findings in a Japanese female patient with a heterozygous *de novo* 15q terminal deletion. The data provide further support for the addition of telomere sequences to truncated chromosome ends, and imply the possible presence of a gene for CHD other than *NR2F2* on distal 15q.

Case Report

This Japanese female patient was born at 39 weeks of gestation after an uncomplicated pregnancy and delivery. At birth, her length was 47.0 cm (–0.7 SD), her weight 2.17 kg (–2.1 SD), and her head circumfer-

Received Aug. 27, 2010; Accepted Dec. 20, 2010 as K10E-251
Released online in J-STAGE as advance publication Jan. 14, 2011

Correspondence to: Sumito Dateki, Department of Molecular Endocrinology, National Research Institute for Child Health and Development, 2-10-1 Ohkura, Setagaya, Tokyo 157-8535, Japan.
E-mail: sdateki@nch.go.jp

Abbreviations: CHD, congenital heart defect; IGF1, insulin-like growth factor 1; IGF1R, insulin-like growth factor 1 receptor; LINE-1, long-interspersed nuclear element-1; MLPA, multiplex ligation-dependent probe amplification; NR2F2, nuclear subfamily group F member 2; VSD, ventricular septal defect.

ence 32.5 cm (–0.5 SD). Although she was found to have ventricular septal defect (VSD), it closed spontaneously at 6 years of age. Menarche occurred at 11 years 6 months of age (menarchial age of Japanese females, 9.75–14.75 years).

At 11 years 9 months of age, she was referred to us because of short stature. Her height was 129. 4 cm (–3.2 SD), and her weight 37.5 kg (–0.6 SD). There were no dysmorphic features. She exhibited mild mental retardation and learning difficulties. Her breast development was at Tanner stage 4 and her pubic hair at Tanner stage 3. Endocrine studies showed an extremely high serum insulin-like growth factor-1 (IGF1) value (1070 ng/mL) (age- and sex-matched reference data, 206–731 ng/mL) and apparently normal serum growth hormone value (2.85 ng/mL) (reference data, 0.32–3.85 ng/mL) and IGF-binding protein-3 value (3.78 μg/mL) (reference data, 2.30–4.39 μg/mL), suggesting the presence of either bioinactive IGF1 or IGF1R resistance in this patient. Her bone age was assessed as 12 years 6 months. On the last examination at 13 years 9 months old, she measured 134.7 cm (–3.9 SD), weighed 45 kg (–0.5 SD), and manifested full pubertal development.

The non-consanguineous parents and three elder brothers were clinically normal. The father was 174 cm (+0.6 SD) tall, and the mother was 151 cm (–1.3 SD) tall.

Molecular Studies

We performed molecular studies using leukocyte DNA samples and lymphocyte metaphase spreads. This study was approved by the Institutional Review Board Committee at National Center for Child Health and Development, and performed after obtaining written informed consent.

We first performed direct sequencing of *IGF1* and *IGF1R* of this patient, identifying no mutation or variation in all the coding exons and their flanking splice sites (the primer sequences are available on request). Thus, multiplex ligation-dependent probe amplification (MLPA) was performed for *IGF1R* using a commercially available MLPA probe mix (P217) (MRC-Holland, Amsterdam), indicating heterozygous deletion of *IGF1R* (Fig. 1A). This deletion was confirmed by FISH with an RP11-262P8 BAC probe detecting a region within *IGF1R* (BACPAC Resources Center, Oakland, CA) (Fig. 1A). To examine the deletion size, oligoarray comparative genomic hybridization was carried out with 1x244K Human Genome Array (catalog No. G4411B) (Agilent Technologies, CA), showing a ~5.0 Mb deletion distal to 15q26.2 (Fig. 1B). Furthermore, to determine the precise deletion junction, we obtained long PCR products with a forward primer hybridizing to a region proximal to the deletion (5'-TAT AACAGACCAAAGCTGGAATGA-3') and a reverse primer complementary to telomere repeat sequences (5'-CTAACCCTAACCCTAACCCTAACC-3'), and examined the sequence of the PCR products with serial primers. Consequently, the breakpoints were determined by direct sequencing with the following primer (5'-GCAATACAAAGACTAGATGCCGTA-3') (Fig. 1B). According to the NCBI Database (NC_000014.7) (http://www.ncbi.nlm.nih.gov/), the deletion was 5,013,940 bp in physical size and was associated with an addition of telomere repeat sequences at the end of the truncated chromosome. The proximal deletion breakpoint was found to reside within a long-interspersed nuclear element-1 element (LINE-1) (subfamily LIME3F) by Repeatmasker (http://www.repeatmasker.org). While this deletion removed 44 genes including *IGF1R*, *NR2F2* was preserved (Ensemble Genome Browser, http://ww.ensemble.org/). Microsatellite analysis for *D15S120* on the deleted region showed that the deletion occurred in the paternally derived chromosome (Fig. 1C). The parents were found to have neither 15q deletion nor reciprocal translocation involving 15q.

Discussion

We identified a heterozygous *de novo* simple 15q26 terminal deletion with telomere sequences. The results provide further support for the notion that terminal truncated deletions are healed by *de novo* addition of telomere repetitive sequences indispensable for chromosome stability and DNA replication. In this regard, the telomerase activity is found in the germline as well as in most cancer cells, but it is generally undetected in normal human somatic tissues [9]. It is likely, therefore, that the chromosomal deletion and the telomere addition took place in the germline.

Phenotypic comparison between this patient and previously reported patients with simple terminal 15q26 deletions [1] provides several useful implications for genotype-phenotype correlations. In this regards, while terminal 15q26 deletions can also occur in complex chromosomal rearrangements such as ring chro-

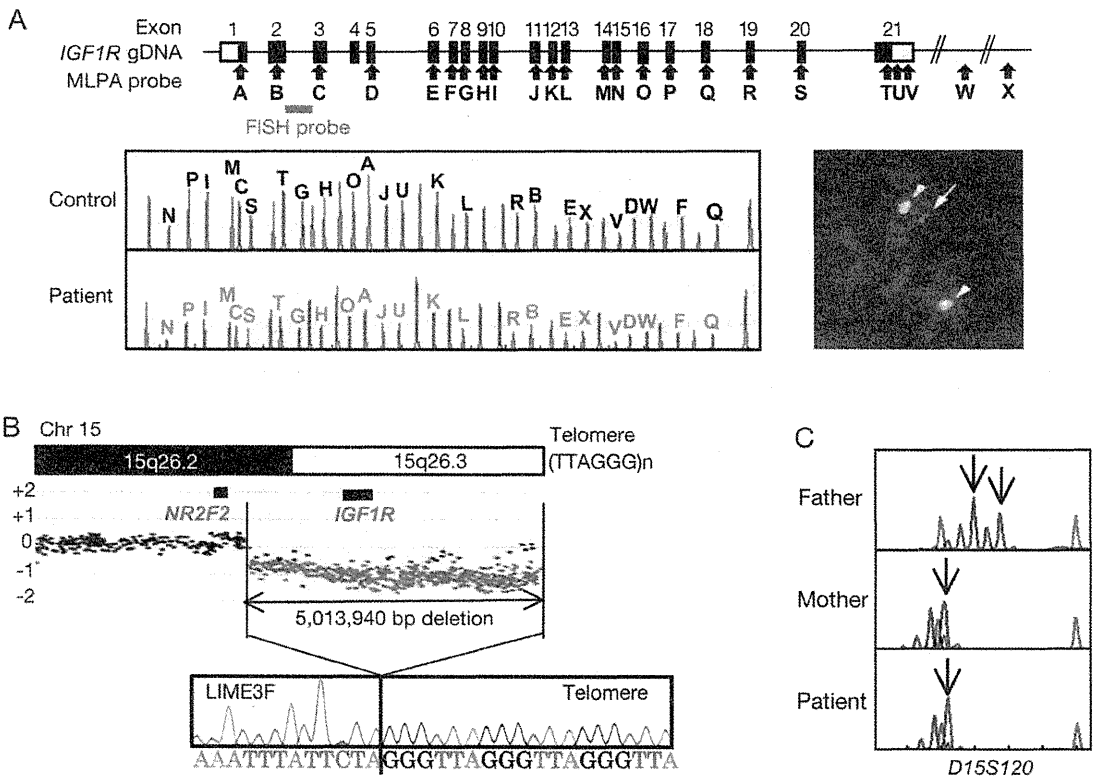

Fig. 1 Deletion analysis.
A MLPA and FISH analyses. The black and white boxes on genomic DNA (gDNA) denote the coding regions and the untranslated regions, respectively. The sites examined by MLPA probes (A–X) are indicated by arrows, and the region detected by an RP11-262P8 BAC FISH probe is shown by a thick horizontal line. In MLPA analysis, the peaks corresponding to sites within the *IGF1R* gene (A–V) and two sites at 2.0 (W) and 2.8 Mb (X) downstream of the *IGF1R* gene are reduced in the patient. In FISH analysis, the probe for *IGF1R* (RP11-262P8) detects only a single signal (an arrow), whereas the CEP 15 (D15Z4) control probe identifies two signals (arrowheads). The probe for *IGF1R* was labeled with digoxigenin and detected by rhodamine anti-digoxigenin, and the CEP 15 probe was detected according to the manufacturer's protocol (Abbott, http://www.abbottmolecular.com/).
B Oligoarray CGH analysis and direct sequencing of the deletion junction. The deletion is 5,013,940 bp in physical size and is associated with an addition of telomere repetitive sequences at the end of the truncated chromosome 15.
C Microsatellite marker analysis. For *D15S120*, one of the maternal alleles is transmitted to the patients, whereas both of the paternal alleles are not transmitted to the patient.

mosome 15 and unbalanced translocation involving 15q26 [12], genotype-phenotype analysis of 15q26 deletion is difficult in complex chromosomal rearrangements because of accompanying chromosomal aberrations.

First, this patient had short stature and mental retardation, as have been observed in most patients with simple terminal 15q26 deletions [1]. This would primarily be ascribed to loss of *IGF1R*, although other genetic and environmental factors may also have some effects. Indeed, heterozygous intragenic *IGF1R* mutations are usually associated with pre-and post-natal growth failure and sometimes accompanied by mental retardation [2, 13–16]. While the birth length of this patient remained within the normal range, this is not necessarily inconsistent with *IGF1R* deletion. It is known that *IGF1R* haploinsufficiency sometimes permit normal birth length and/or weight [1]. Similarly, while the serum IGF1 level was markedly elevated in this patient, this would basically be compatible with *IGF1R* deletion. It is known that serum IGF1 levels tend to be elevated in patients with *IGF1R* haploinsufficiency [1, 2]. To our knowledge, however, such a high serum IGF1 level has not been reported to date. Thus, although underlying factor(s) for the extremely high IGF1 level remains to be clarified, the present data indicate that serum IGF1 level can be markedly elevated in patients with *IGF1R* haploinsufficiency.

Second, she also had CHD (VSD) that is often identified in patients with simple terminal 15q26 deletions [1, 4–6]. In this regard, although previous genotype-phenotype correlations in patients with 15q26 deletions and knockout mice studies argue that loss of *NR2F2* may lead to various types of CHD with incomplete penetrance [3–6], *NR2F2* was preserved in this patient. In addition, the development of CHD is obviously inexplicable by *IGF1R* deletion [1, 2]. Thus, it might be possible that a hitherto unknown gene(s) for CHD (VSD) with variable expressivity and penetrance resides on the deleted region, although CHD (VSD) could be a co-incidental feature independent of the deletion or a non-specific feature common to various chromosomal abnormalities [17–19]. Furthermore, loss of the putative gene may also be relevant to the development of CHD in the previously reported patients with 15q26 deletions [4–6].

Lastly, she had no other clinically discernible features, while most patients with simple 15q26 terminal deletions have additional features such as diaphragmatic hernia, renal anomalies, club feet, oculocutaneous albinism, and seizure [1]. However, such features have been observed in a single or only a few patients with apparently large simple terminal 15q26 deletions. Thus, such features could be regarded as developmental insults that became recognizable by chromosome imbalance [18, 19]. This notion would be supported by the fact that such additional features are more frequently found in complex chromosomal rearrangements involving 15q26 than in simple terminal 15q deletions [1, 12], because chromosomal imbalance is more severe in complex chromosomal rearrangements. In addition, if a gene(s) for such features is present on distal 15q, it is likely that such a gene(s) was preserved in this patient with a relatively small deletion, or that loss of the gene(s) did not cause clinically discernible phenotypes in this patient because of low penetrance.

In summary, the results provide further evidence for the addition of telomere sequences to truncated chromosome ends, and suggest the possible presence of a gene for CHD other than *NR2F2* on distal 15q. Furthermore, it is recommended to examine 15q deletions in patients with clinical features indicative of *IGF1R* abnormality (growth failure with relatively to obviously high serum IGF1, and mental retardation) and other phenotypes including CHD.

Acknowledgements

This study was supported by Grants for Child Health and Development (20C-2) and Research on Children and Families (H21-005) from the Ministry of Health, Labor, and Welfare, and by Grants from the Ministry of Education, Culture, Sports, Science, and Technology, Japan.

Appendix

The authors have nothing to declare.

References

1. Ester WA, van Duyvenvoorde HA, de Wit CC, Broekman AJ, Ruivenkamp CA, Govaerts LC, Wit JM, Hokken-Koelega AC, Losekoot M (2009) Two short children born small for gestational age with insulin-like growth factor 1 receptor haploinsufficiency illustrate the heterogeneity of its phenotype. *J Clin Endocrinol Metab* 94: 4717-4727.
2. Walenkamp MJ, Wit JM (2008) Single gene mutations causing SGA. *Best Pract Res Clin Endocrinol Metab* 22: 433-446.
3. Pereira FA, Qiu Y, Zhou G, Tsai MJ, Tsai SY (1999) The orphan nuclear receptor COUP-TFII is required for angiogenesis and heart development. *Genes Dev* 13: 1037-1049.
4. Pinson L, Perrin A, Plouzennec C, Parent P, Metz C, Collet M, Le Bris MJ, Douet-Guilbert N, Morel F, De Braekeleer M (2005) Detection of an unexpected subtelomeric 15q26.2 --> qter deletion in a little girl: clinical and cytogenetic studies. *Am J Med Genet A* 138A: 160-165.
5. Poot M, Eleveld MJ, van 't Slot R, van Genderen MM, Verrijn Stuart AA, Hochstenbach R, Beemer FA (2007) Proportional growth failure and oculocutaneous albinism in a girl with a 6.87 Mb deletion of region 15q26.2-->qter. *Eur J Med Genet* 50: 432-440.
6. Rump P, Dijkhuizen T, Sikkema-Raddatz B, Lemmink HH, Vos YJ, Verheij JB, van Ravenswaaij CM (2008) Drayer's syndrome of mental retardation, microcephaly, short stature and absent phalanges is caused by a recurrent deletion of chromosome 15(q26.2-->qter). *Clin Genet* 74: 455-462.
7. Moyzis RK, Buckingham JM, Cram LS, Dani M, Deaven LL, Jones MD, Meyne J, Ratliff RL, Wu JR (1988) A highly conserved repetitive DNA sequence,

(TTAGGG)n, present at the telomeres of human chromosomes. *Proc Natl Acad Sci U S A* 85: 6622-6626.
8. Shippen-Lentz D, Blackburn EH (1990) Functional evidence for an RNA template in telomerase. *Science* 247: 546-552.
9. Wright WE, Piatyszek MA, Rainey WE, Byrd W, Shay JW (1996) Telomerase activity in human germline and embryonic tissues and cells. *Dev Genet* 18: 173-179.
10. Varley H, Di S, Scherer SW, Royle NJ (2000) Characterization of terminal deletions at 7q32 and 22q13.3 healed by De novo telomere addition. *Am J Hum Genet* 67: 610-622.
11. Yatsenko SA, Brundage EK, Roney EK, Cheung SW, Chinault AC, Lupski JR (2009) Molecular mechanisms for subtelomeric rearrangements associated with the 9q34.3 microdeletion syndrome. *Hum Mol Genet* 18: 1924-1936.
12. Klaassens M, Galjaard RJ, Scott DA, Brüggenwirth HT, van Opstal D, Fox MV, Higgins RR, Cohen-Overbeek TE, Schoonderwaldt EM, Lee B, Tibboel D, de Klein A (2007) Prenatal detection and outcome of congenital diaphragmatic hernia (CDH) associated with deletion of chromosome 15q26: two patients and review of the literature. *Am J Med Genet A* 143A: 2204-2212.
13. Abuzzahab MJ, Schneider A, Goddard A, Grigorescu F, Lautier C, Keller E, Kiess W, Klammt J, Kratzsch J, Osgood D, Pfäffle R, Raile K, Seidel B, Smith RJ, Chernausek SD; Intrauterine Growth Retardation (IUGR) Study Group (2003) IGF-I receptor mutations resulting in intrauterine and postnatal growth retardation. *N Engl J Med* 349: 2211-2222.
14. Kawashima Y, Kanzaki S, Yang F, Kinoshita T, Hanaki K, Nagaishi J, Ohtsuka Y, Hisatome I, Ninomoya H, Nanba E, Fukushima T, Takahashi S (2005) Mutation at cleavage site of insulin-like growth factor receptor in a short-stature child born with intrauterine growth retardation. *J Clin Endocrinol Metab* 90: 4679-4687.
15. Wallborn T, Wüller S, Klammt J, Kruis T, Kratzsch J, Schmidt G, Schlicke M, Müller E, van de Leur HS, Kiess W, Pfäffle R (2010) A heterozygous mutation of the insulin-like growth factor-I receptor causes retention of the nascent protein in the endoplasmic reticulum and results in intrauterine and postnatal growth retardation. *J Clin Endocrinol Metab* 95: 2316-2324.
16. Kruis T, Klammt J, Galli-Tsinopoulou A, Wallborn T, Schlicke M, Müller E, Kratzsch J, Körner A, Odeh R, Kiess W, Pfäffle R (2010) Heterozygous mutation within a kinase-conserved motif of the insulin-like growth factor I receptor causes intrauterine and postnatal growth retardation. *J Clin Endocrinol Metab* 95: 1137-1142.
17. Jones KL (2006) Smith's recognizable patterns of human malformations. 6th edn. Elisevier Saunders, Philadelphia.
18. Gilbert EF, Opitz JM (1982) Developmental and other pathologic changes in syndromes caused by chromosome abnormalities. *Perspect Pediatr Pathol* 7: 1-63.
19. Epstein CJ (1986) The consequences of chromosome imbalance: principles, mechanisms, and models. Cambridge University Press. Cambridge.

Pediatr Radiol (2011) 41:1013–1019
DOI 10.1007/s00247-011-2132-1

ORIGINAL ARTICLE

Radiological evaluation of dysmorphic thorax of paternal uniparental disomy 14

Osamu Miyazaki · Gen Nishimura · Masayo Kagami · Tsutomu Ogata

Received: 21 November 2010 / Revised: 31 January 2011 / Accepted: 1 February 2011 / Published online: 24 May 2011

Abstract
Background The "coat-hanger" sign of the ribs with a bell-shaped thorax has been known as a radiological hallmark of the paternal uniparental disomy 14 (upd(14)pat).
Objective To quantitatively determine the differences in thoracic deformity between upd(14)pat and other bone diseases with thoracic hypoplasia and to establish the age-dependent evolution.
Materials and methods The subjects comprised 11 children with upd(14)pat. The angle between the 6th posterior rib and the horizontal axis was measured (coat hanger angle; CHA). The ratio of the mid- to widest thorax diameter (M/W ratio) was calculated for the bell-shaped thorax.
Results CHA ranged from +28.5 to 45° (mean; 35.1°±5.2) in upd(14)pat, and from −19.8 to 21° (−3.3±13°) in bone dysplasias ($p<0.01$). The M/W ratio ranged from 58% to 93% (75.4±10) in upd(14)pat, and from 80% to 92% (86.8±3.3) in bone dysplasias ($p<0.05$). Serial radiographs revealed that CHA remained constant during early childhood, while the M/W ratio gradually increased with age.
Conclusion The "coat-hanger" sign of upd(14)pat provides a distinctive radiological gestalt that makes it possible to differentiate the disorder from other skeletal dysplasias. By contrast, the bell-shaped thorax is significant only in the neonatal period.

Keywords UPD14 · Plain radiograph · Coat-hanger sign · Bell-shaped thorax

O. Miyazaki (✉)
Department of Radiology,
National Center for Child Health and Development,
2-10-1 Okura,
Seatagaya-ku, Tokyo 157-8535, Japan
e-mail: osamu-m@rc4.so-net.ne.jp

G. Nishimura
Department of Radiology,
Tokyo Metropolitan Children's Medical Center,
2-8-29 Musashidai,
Fuchu-shi, Tokyo 183-8561, Japan

M. Kagami · T. Ogata
Division of Clinical Genetics and Molecular Medicine,
National Center for Child Health and Development,
2-10-1 Okura,
Seatagaya-ku, Tokyo 157-8535, Japan

Introduction

Uniparental disomy (UPD) refers to the inheritance of a pair of chromosomes from only one parent. UPD is a relatively common phenomenon. The inheritance of both, or parts of both, maternal chromosomes (heterodisomic maternal UPD) has been found to become more prevalent as parental age becomes more advanced [1]. It is well established that UPD for chromosomes 6, 7, 11, 14 and 15 is associated with recognized syndromes, including Prader-Willi syndrome (maternal UPD 15), Angelman syndrome (paternal UPD 15), and Beckwith-Wiedemann syndrome (paternal UPD 11) [2].

The paternal UPD 14 phenotype (upd(14)pat) is a recently recognized genetic condition that is caused by an aberration of the imprinting center in chromosome 14. The clinical hallmarks of upd(14)pat are thoracic hypoplasia and abdominal wall defect. Mild facial dysmorphism and developmental delay are also noted. In addition, upd(14)pat presents with a distinctive radiological finding: the "coat-hanger" appearance of the ribs and a bell-shaped thorax [3]. In the past, upd(14)pat was often misdiagnosed as bone dysplasias with thoracic hypoplasia, as in Jeune syndrome [4], because attention was not paid to the morphological differences of the thorax between upd(14)pat and other genetic bone diseases. Previous reports on

upd(14)pat have been based on a single case or a limited number of cases. To date, there has been no radiological report involving a large series of upd(14)pat cases. Although a previous report suggested that the dysmorphic thorax in upd(14)pat ameliorated in the mid-childhood period [5], it remains to be determined how the thoracic deformity in upd (14)pat evolves with age. The purpose of this study was to quantitatively determine the differences in the thoracic deformity between upd(14)pat and other genetic bone diseases, and to establish the age-dependent radiological evolution of the thoracic hypoplasia in upd(14)pat.

Materials and methods

The subjects comprised 11 children (6 girls and 5 boys) with upd(14)pat phenotypes proven on molecular grounds [5, 6]. Three of the 11 children had been managed in our hospital, and 8 were referred to our institution for molecular diagnosis. The molecular diagnoses included seven cases of paternal uniparental disomy, two of microdeletion and two of epimutation. The initial radiographs available for the analysis were obtained in the neonatal period (n=8), and at 7, 24 and 32 months of age (n=1). Sequential radiological evaluation was feasible in 4 of 11 children up to 5 years of age. The study was approved by the institutional review board at the National Center for Child Health and Development.

To assess for the "coat-hanger" sign, the angle between the 6th posterior rib and the horizontal axis was measured (coat hanger angle, CHA; an upward angle was defined as +, and a downward angle as −). The ratio of the mid- to widest thorax diameter (M/W ratio) was calculated for the bell-shaped thorax (Figs. 1, 2). For comparison, both indexes were evaluated in nine cases with bone dysplasia with thoracic hypoplasia, including thanatophoric dysplasia (n=6), Ellis-van Creveld syndrome (n=2) and asphyxiating thoracic dysplasia (n=1). These cases were selected from our radiology database. The children's ages ranged from 21 weeks of gestation to 6 years of age (mean: 11 months of age). Both indexes were also evaluated in five children with respiratory distress syndrome (RDS) and without skeletal abnormalities that could be assessed to determine the evolution of the normal thoracic morphology. In the RDS group, serial follow-up radiographs were available from the neonatal period up to 2 years to 6 years of age (mean 4.2). The measurement of CHA and M/W ratio was performed using an accessory digital tool from a PACS

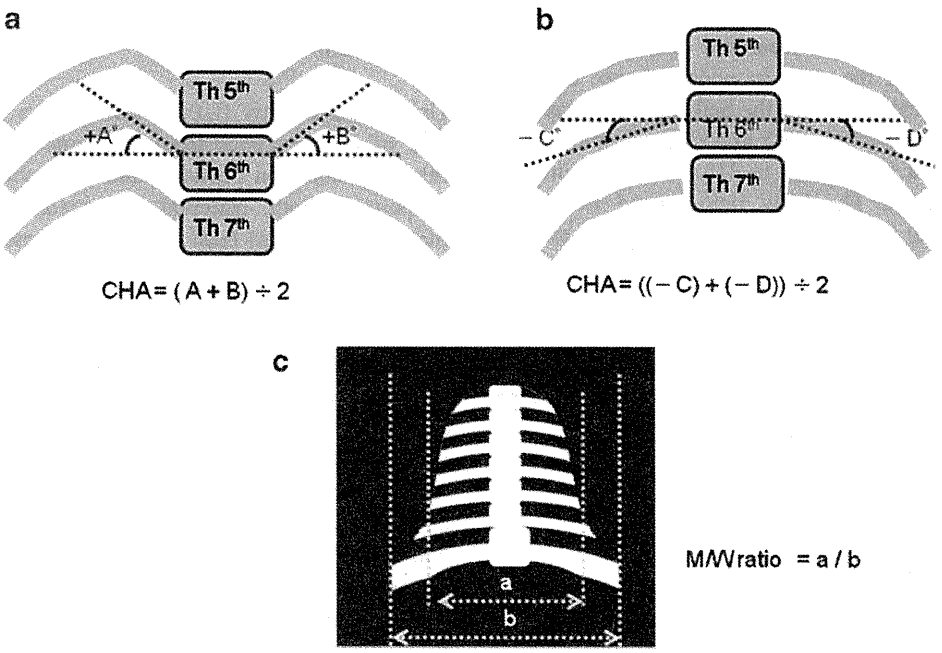

Fig. 1 **a**, **b** Diagram of coat-hanger angle (CHA) and mid/widest ratio. CHA refers to the average of the angles between the peak point of both 6th posterior ribs and the horizontal axis. If there is no peak point of the 6th posterior ribs, the center of the ribs is utilized instead. The horizontal axis is defined as a line passing through two points of both 6th cost-vertebral junctions. An upward angle is defined as +, and a downward angle as −. CHA is thought to be a quantitative index of the coat-hanger sign. **c** The ratio of mid- to widest thorax (M/W ratio) refers to the ratio of the narrowest diameter of the mid-thorax to the widest diameter of the basal thorax. In most cases with upd(14)pat, the thorax showed medial concavity with the top of approximately the 6th rib (the narrowest mid-thorax) and downward sloping toward the 9th to 11th ribs (the widest basal thorax). M/W ratio is thought to be a quantitative index of dysmorphic bell-shaped thorax

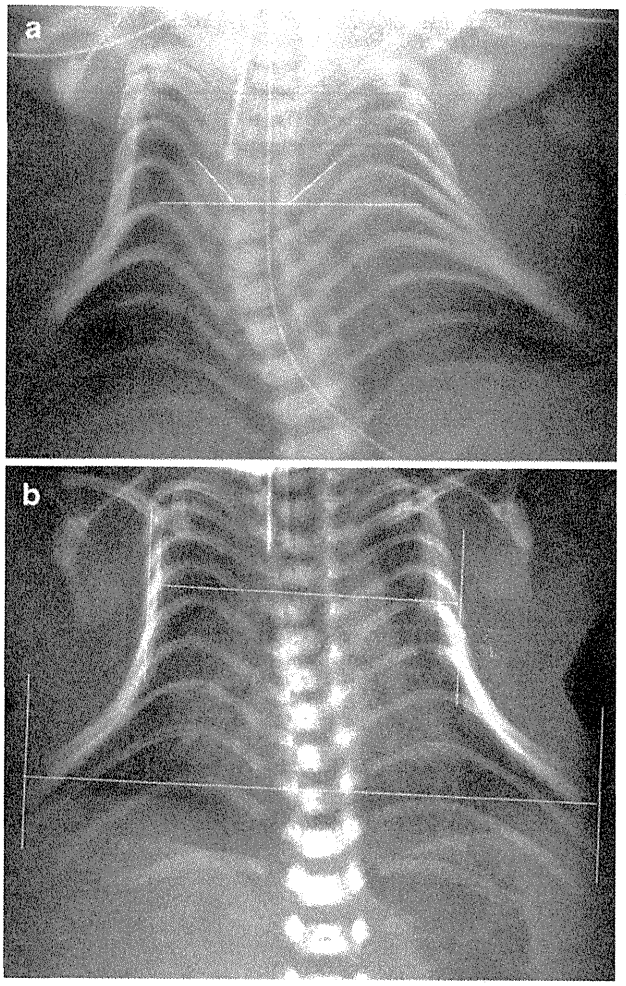

Fig. 2 Examples of CHA and M/W ratio. **a** The 6th posterior ribs show upward bowing that provides the coat-hanger sign. The CHA of this case (patient #7 in Table 1) was 45° (the measurement was 48° for the right and 42° for the left). **b** The M/W ratio was 58% in this case (patient #5 in Table 1). This is an example of severe bell-shaped thorax in upd(14)pat

system (Centricity ™ RA 1000 Ver.3.0, GE Healthcare, Milwaukee, WI) on the PACS monitor, or using area and protractor commercial software (Lenara Ver2.21, Vector, Tokyo) on a personal computer monitor. An unpaired two-tailed t-test was used for statistical evaluation.

Results

Clinical and measurement data are summarized in Table 1 and Fig. 3. All 11 children with upd(14)pat showed a severe upward sweep of the posterior rib or increased CHA, ranging from +28.5 to 45° (mean ± SD; 35.1°±5.2) (Figs. 2, 3). Children with bone dysplasias presented with variable manifestations of the posterior rib, and CHA ranged from −19.8 to 21° (mean ± SD; −3.3±13°) (Figs. 3, 4). The difference in CHA was statistically significant between the upd(14)pat and bone dysplasia groups ($P<0.01$). According to this result, approximately +25° was the estimated cut-off line of CHA to differentiate upd(14)pat from skeletal dysplasias (Fig. 3). The M/W ratio ranged from 58% to 93% (mean±SD; 75.4±10) in the upd(14)pat group, while it ranged between 80% and 92% (mean±SD; 86.8±3.3) in the skeletal dysplasia group (Fig. 3). The difference an unpaired two-tailed t-test in the M/W ratio was, though statistically significant, less conspicuous than that in CHA ($P<0.05$). There was considerable overlap in the range of the M/W ratio between the upd(14)pat and skeletal dysplasia groups.

The age-dependent evolution of CHA and M/W ratio in the upd(14)pat and RDS groups is shown in Fig. 5. In the four children with upd(14)pat, CHA remained unaltered regardless of age, ranging from 25° to 45°. In the RDS group ($n=5$), CHA was constant regardless of age, ranging from −6.4 to 10° (mean −0.6) at birth and from −8 to 7.3° thereafter (Fig. 5). The M/W ratio of the upd(14)pat group was smaller than that of the RDS group in the neonatal period. However, it increased gradually with age and finally caught up with that observed in the RDS group (Figs. 6, 7).

Discussion

The clinical manifestations of upd(14)pat have been well established to date. The hallmarks of this condition include a small thorax, laryngomalacia, hypoplastic abdominal wall, short limbs with joint contractures, craniofacial dysmorphism, and mental retardation [2]. In addition, several reports on the prenatal diagnosis of upd(14)pat suggested the common occurrence of polyhydramnios and preterm delivery in upd(14)pat [2, 7]. A few reports on upd (14)pat have detailed the radiological manifestations, such as disproportionately short limbs, spurring of lower femoral and upper tibial metaphyses, absent glenoid fossa, shortened iliac wing with flaring, thin and elongated clavicle, hypoplastic scapular neck, kyphoscoliosis, hypoplasia of the maxilla and mandible, a broad nasal bridge, wide sutures and multiple wormian skull bones, contractures of the wrists with ulnar deviation, and stippled calcification [3, 8–10]. However, these findings are so mild that alone they do not determine the diagnosis. Instead, the distinctive thoracic deformity in upd(14)pat, termed the coat-hanger sign as introduced by Offiah et al. [3], enables a definitive diagnosis to be made. Sutton et al. [8] described the thoracic deformity of upd(14)pat as "anterior ribs bowed caudally (downward), and posterior portions of the ribs bowed cranially (upward)," and these configurations are combined in the characteristic coat-hanger sign of the ribs

Table 1 Summary of clinical details, measurement of rib angle, coat-hanger angle (CHA), and ratio of mid- to widest thorax (M/W ratio). *GW* gestational week, *TD* thanatophoric dysplasia, *ATD* asphyxiating thoracic dysplasia, *EvC* Ellis-van Creveld syndrome, *RDS* respiratory distress syndrome

Case	Gender	Age (months)[a]	Molecular or clinical diagnosis	Right rib angle (°)	Left rib angle (°)	CHA (°)	M/W ratio (%)
upd(14)pat patients							
1	f	0	upd	36	31	33.5	80
2	m	0	upd	43	41	42	66
3	m	0	upd	27	46	36.5	80
4	m	7	upd	32	38	35	80
5	m	0	deletion	27	30	28.5	58
6	f	0	Epimutation	35	23	29	77
7	f	0	Epimutation	48	42	45	65
8	f (45,XX)	0	upd	30	34	32	69
9	f	0	upd	46	32	39	74
10	m	24	upd	28	38	33	87
11	f	32	decision	32	33	32.5	93
mean		5.7		35	35.82	35.1	75.4
TD group patients							
1	m	21GW	TD	−9.9	−13.7	−11.8	80
2	f	6	TD	−3.7	12	1	85.6
3	m	21GW	TD	−11.7	−13.9	−12.8	86
4	Unknown	20GW	TD	−19.6	−20	−19.8	86
5	m	0	TD	7	−12	−2.5	87
6	m	21GW	TD	−15	−21	−18	87
7	m	84	ATD	4	2	3	88
8	f	11	EvC	9.6	10.3	9.95	90
9	m	24	EvC	14	28	21	92
mean		11		−2.8	−3.1	−3.3	86.8
RDS patients							
1	m	0	RDS	1.8	4	2.9	90
2	m	0	RDS	1.2	−14	−6.4	81.7
3	m	0	RDS	−6.9	−4.1	−5.2	84
4	m	0	RDS	−6	−2	−4	91
5	f	0	RDS	11.3	8.7	10	85
mean		0		0.28	−1.48	−0.54	86.3

[a] Age at which time the initial radiograph was available

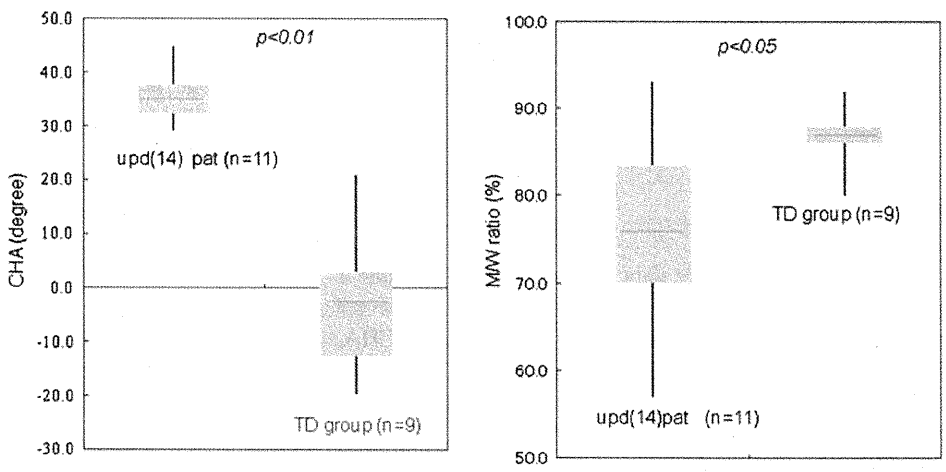

Fig. 3 Box plot of CHA and M/W ratio with the median, interquartile interval and range

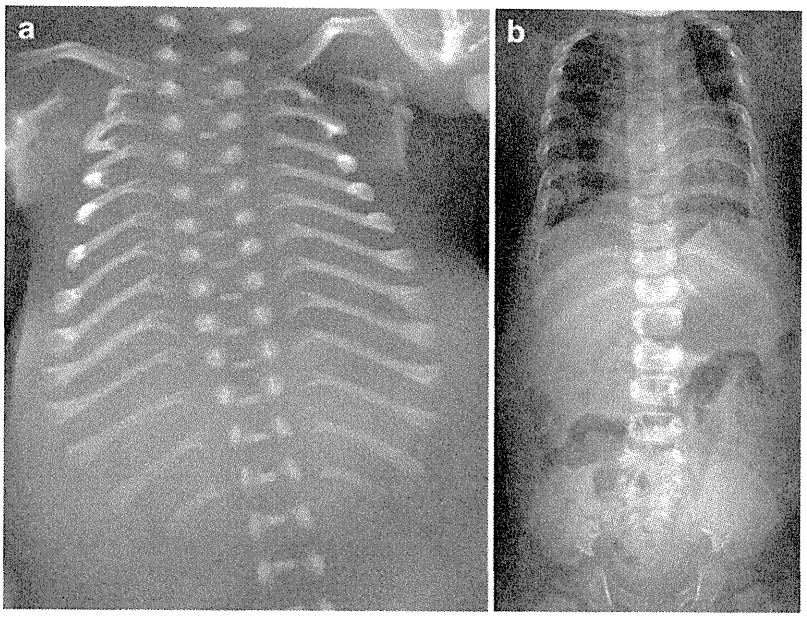

Fig. 4 Examples of the thoracic appearance and measurement of bone dysplasias with thoracic hypoplasia. **a** Thanatophoric dysplasia (TD) type 1 (stillbirth at 21 weeks of gestation). Note a narrow thorax with cupped anterior ends as well as short long bones with metaphyseal cupping. The posterior ribs show downward sloping. The CHA was −18°, and the M/W ratio was 87%. Despite the presence of severe thoracic hypoplasia in TD, its morphology is different from that seen in upd(14)pat (Fig. 2). **b** Ellis-van Creveld (EvC) syndrome (2 years of age). The thorax appears narrow, and a trident appearance of the acetabula is seen. Posterior ribs show upward sloping. The CHA was 21°, and the M/W ratio was 92%. The morphological pattern of the thorax differs from that of upd(14)pat

on the chest radiograph. Sutton et al. concluded that the skeletal phenotype in upd(14)pat involves primarily the axial skeleton, with little to no effect on the long bones. Very small changes of the long bones in upd(14)pat correspond with those of the mouse model (UPD of the distal segment of mouse chromosome 12) [11]. Consequently, it is assumed that imprinted genes on human chromosome 14 and mouse chromosome 12 play a role in axial skeletal formation and ossification [8, 11].

In the subsequent articles on upd(14)pat, all 11 affected children presented unexceptionally with the coat-hanger sign [5, 6, 12]. It was thought that the upward posterior rib bowing and downward anterior rib bowing (the coat-hanger appearance) in upd(14)pat contrast with the horizontally oriented ribs generally seen in disorders with thoracic hypoplasia. Based on the radiological sign, along with other radiological findings, it is not difficult to differentiate upd(14)pat from other genetic disorders involv-

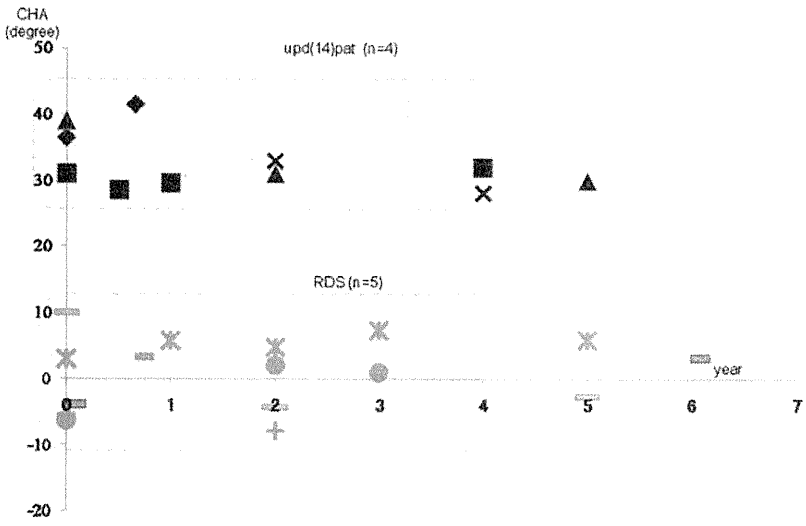

Fig. 5 Comparative observation of age-dependent transition of CHA between the upd(14)pat and respiratory distress syndrome (RDS) groups. Individual shapes represent individual patients

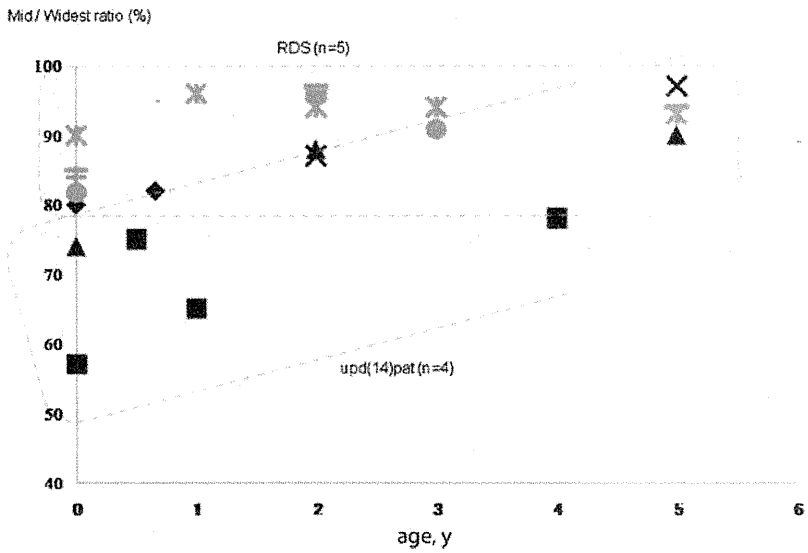

Fig. 6 Comparative observation of age-dependent transition of M/W ratio between the upd(14) pat and RDS groups. Individual shapes represent individual patients

ing thoracic hypoplasia, such as thanatophoric dysplasia, asphyxiating thoracic dysplasia and metatropic dysplasia [13]. However, there are several disorders wherein thoracic hypoplasia is the sole radiological hallmark, including Barnes syndrome, Shwachman-Diamond syndrome and the mildest cases of asphyxiating thoracic hypoplasia. Thus, we thought that quantitative analyses of the coat-hanger sign could elucidate how different the thoracic hypoplasia

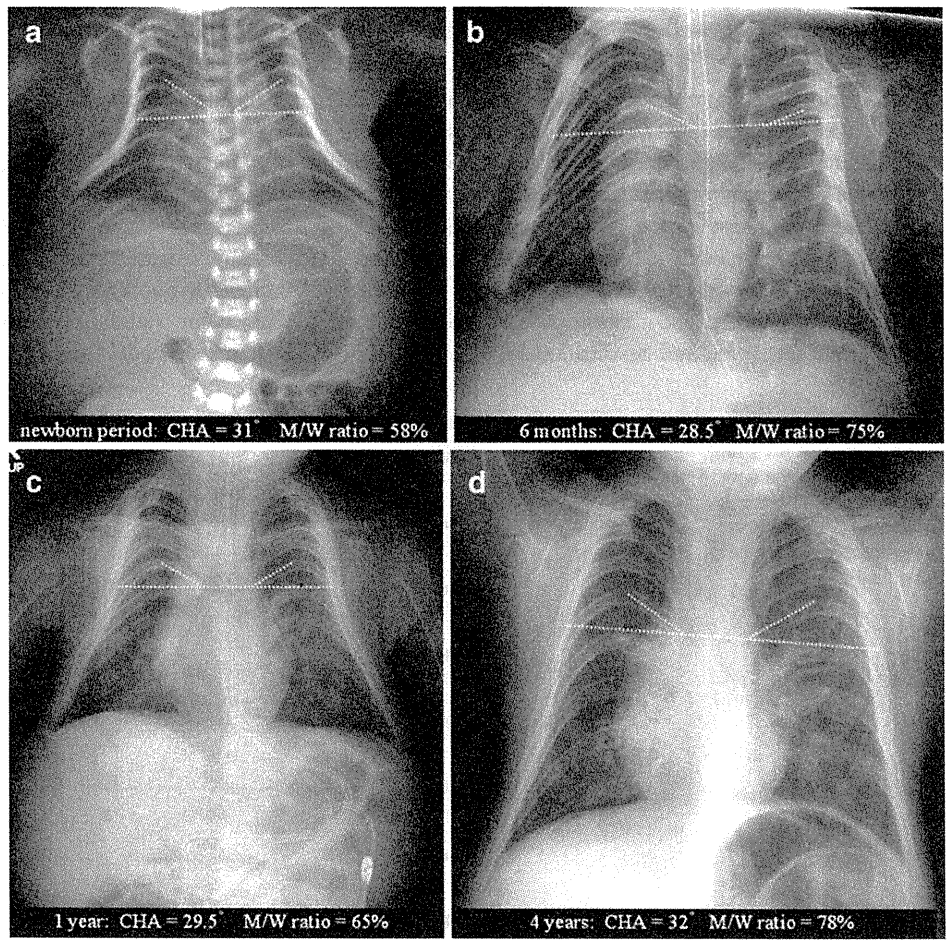

Fig. 7 Serial images of the thorax deformity in upd(14)pat. In this case, four images taken at different ages were available: (**a**) neonatal period, (**b**) 6 months, (**c**) 1 year and (**d**) 4 years. The CHA was almost consistent regardless of age, while the M/W ratio increased with advancing age. The coat-hanger sign and bell-shaped thorax are readily identifiable in the neonatal period. The diagnosis is not straightforward in childhood, yet close observation combined with CHA measurement points to the coat-hanger sign

in upd(14)pat is from the thoracic hypoplasia in other genetic disorders, and presumed that the measurement of CHA (mean 35.1°) and M/W ratio (mean 75.4%) might be helpful when the diagnosis of upd(14)pat is in question. As comparison groups, we included not only cases of severe bone dysplasias but also RDS. Neonates with RDS may present with a small chest [14], and it is not uncommon for them to undergo repeated examinations of chest radiographs because of the association with chronic lung disease.

Kagami et al. [5] reported the age-dependent evolution of the thoracic deformity of upd(14)pat in two children, which was said to ameliorate in mid-childhood. Their observation corresponded with the improvement of the M/W ratio with age described here. By contrast, however, CHA persisted consistently until mid-childhood. This finding indicates that the coat-hanger sign is still discernable during mid-childhood. Radiological findings are presumed to be the only clue to the presence of upd(14)pat after mid-childhood. Serial radiographs (newborn, 2 years and 9 years), as illustrated by Cotter et al. [15] also warrant our observation.

A drawback of this study is that it includes a limited number of cases and available radiographs with uneven quality, such as chest radiographs with some obliquity and radiographs taken in the supine position in the neonatal period vs. the upright position in childhood. Even taking into account these technical problems, however, we believe that our quantitative analyses, particularly the measurement of the CHA, are a valid way to characterize the distinctive thoracic deformity in upd(14)pat.

Conclusion

The coat-hanger sign of upd(14)pat was quantitatively represented by CHA, and was found to be more severe than that seen in other genetic bone diseases and to persist into early childhood; thus, the findings will help in the diagnosis of upd(14)pat even after infancy. By contrast, the bell-shaped thorax represented by M/W ratio was significant only in the neonatal period, and its diagnostic value declined with age.

References

1. Kotzot D (2004) Advanced parental age in maternal uniparental disomy (UPD): implication for the mechanism of formation. Eur J Hum Genet 12:343–346
2. Towner D, Yang SP, Shaffer G (2001) Prenatal ultrasound findings in a fetus with paternal uniparental disomy 14q12-qter. Ultrasound Obstet Gynecol 18:268–271
3. Offiah AC, Cornette L, Hall CM (2003) Paternal uniparental disomy 14: introducing the "coat-hanger" sign. Pediatr Radiol 33:509–512
4. Stevenson DA, Brothman AR, Chen Z et al (2004) Paternal uniparental disomy of chromosome 14: confirmation of a clinically-recognizable phenotype. Am J Med Genet A 130A:88–91
5. Kagami M, Nishimura G, Okuyama T et al (2005) Segmental and full paternal isodisomy for chromosome 14 in three patients: narrowing the critical region and implication for the clinical feature. Am J Med Genet A 138A:127–132
6. Kurosawa K, Sasaki H, Yamanaka M et al (2002) Paternal UPD 14 is responsible for a distinctive malformation complex. Am J Med Genet 110:268–272
7. Yamanaka M, Ishikawa H, Saito K et al (2010) Prenatal findings of paternal uniparental disomy 14: report of four patients. Am J Med Genet 152A:789–791
8. Sutton VR, McAlister WH, Bertin TK et al (2003) Skeletal defect in paternal uniparental disomy for chromosome 14 are re-capitulated in the mouse model (paternal uniparental disomy 12). Hum Genet 113:447–451
9. Mattes J, Whitehead B, Liehr T et al (2007) Paternal uniparental isodisomy for chromosome 14 with mosaicism for a supernumerary marker chromosome 14. Am J Med Genet 143A:2165–2171
10. Irving MD, Bulting K, Kanber D et al (2010) Segmental paternal uniparental disomy (patUPD) of 14q32 with abnormal methylation elicites the characteristic features of complete pat UPD14. Am J Med Genet 152A:1942–1950
11. Georgiades P, Watkins M, Surani MA et al (2000) Parental origin-specific developmental defects in mice with uniparental disomy for chromosome 12. Development 127:4719–4728
12. Kagami M, Sekita Y, Nishimura G et al (2008) Deletions and epimutations affecting the human 14q32.2 imprinted region in individuals with paternal and maternal upd(14)-like phenotypes. Nat Genet 40:237–242
13. Spranger JW (2002) Asphyxiating thoracic dysplasia. In: Spranger JW, Brill PW, Poznanski A (eds) Bone dysplasia, an atlas of genetic disorders of skeletal development, 2nd edn. Oxford University Press, New York, pp 125–129
14. Swischuk LW (2004) Chapter 1. Respiratory system; respiratory distress in the newborn. In: Swischuk LE (ed) Imaging of the newborn, infant, and young child, 5th edn. Lippincott, Williams & Wilkins, Philadelphia, pp 29–36
15. Cotter PD, Kaffe S, McCurdy LD et al (1997) Paternal uniparental disomy for chromosome 14: a case report and review. Am J Med Genet 70:74–79

Journal of Human Genetics (2010) 55, 801–809

www.nature.com/jhg

ORIGINAL ARTICLE

Mutation analysis of the *SHOC2* gene in Noonan-like syndrome and in hematologic malignancies

Shoko Komatsuzaki[1], Yoko Aoki[1], Tetsuya Niihori[1], Nobuhiko Okamoto[2], Raoul CM Hennekam[3,4], Saskia Hopman[5], Hirofumi Ohashi[6], Seiji Mizuno[7], Yoriko Watanabe[8], Hotaka Kamasaki[9], Ikuko Kondo[10], Nobuko Moriyama[11], Kenji Kurosawa[12], Hiroshi Kawame[13], Ryuhei Okuyama[14], Masue Imaizumi[15], Takeshi Rikiishi[16], Shigeru Tsuchiya[16], Shigeo Kure[1,16] and Yoichi Matsubara[1]

Noonan syndrome is an autosomal dominant disease characterized by dysmorphic features, webbed neck, cardiac anomalies, short stature and cryptorchidism. It shows phenotypic overlap with Costello syndrome and cardio-facio-cutaneous (CFC) syndrome. Noonan syndrome and related disorders are caused by germline mutations in genes encoding molecules in the RAS/MAPK pathway. Recently, a gain-of-function mutation in *SHOC2*, p.S2G, has been identified as causative for a type of Noonan-like syndrome characterized by the presence of loose anagen hair. In order to understand the contribution of *SHOC2* mutations to the clinical manifestations of Noonan syndrome and related disorders, we analyzed *SHOC2* in 92 patients with Noonan syndrome and related disorders who did not exhibit *PTPN11*, *KRAS*, *HRAS*, *BRAF*, *MAP2K1/2*, *SOS1* or *RAF1* mutations. We found the previously identified p.S2G mutation in eight of our patients. We developed a rapid detection system to identify the p.S2G mutation using melting curve analysis, which will be a useful tool to screen for the apparently common mutation. All the patients with the p.S2G mutation showed short stature, sparse hair and atopic skin. Six of the mutation-positive patients showed severe mental retardation and easily pluckable hair, and one showed leukocytosis. No *SHOC2* mutations were identified in leukemia cells from 82 leukemia patients. These results suggest that clinical manifestations in *SHOC2* mutation-positive patients partially overlap with those in patients with typical Noonan or CFC syndrome and show that easily pluckable/loose anagen hair is distinctive in *SHOC2* mutation-positive patients.
Journal of Human Genetics (2010) **55,** 801–809; doi:10.1038/jhg.2010.116; published online 30 September 2010

Keywords: cardio-facio-cutaneous syndrome; costello syndrome; hematologic malignancy; loose anagen hair; melting curve analysis; noonan syndrome

INTRODUCTION

Noonan syndrome (MIM 163950) is an autosomal dominant disorder characterized by short stature, webbed or short neck, characteristic features (hypertelorism, low-set ears and ptosis), pulmonary valve stenosis and hypertrophic cardiomyopathy.[1,2] Noonan syndrome is a heterogeneous disease and overlaps phenotypically with Costello syndrome (MIM 218040) and cardio-facio-cutaneous (CFC) syndrome (MIM 115150). Costello syndrome is characterized by mental retardation, distinctive facial features, neonatal feeding difficulties, curly hair, loose skin, and hypertrophic cardiomyopathy and carries an increased risk of malignancy.[3] CFC syndrome, on the other hand, is characterized by mental retardation, ectodermal abnormalities (sparse hair, hyperkeratotic skin and ichthyosis), distinctive facial features (high forehead, bitemporal constriction, hypoplastic supraorbital ridges, downslanting palpebral fissures and depressed nasal bridge) and congenital heart defects (pulmonic stenosis, atrial septal defect and hypertrophic cardiomyopathy).[4]

Recent studies have shown that all three of these disorders result from dysregulation of the RAS/MAPK cascade. It has been suggested that these syndromes be comprehensively termed the RAS/MAPK syndromes[5] or the neuro-cardio-facial-cutaneous syndrome.[6] Germline mutations in *PTPN11*, *KRAS*, *SOS1* and *RAF1* have been

[1]Department of Medical Genetics, Tohoku University School of Medicine, Sendai, Japan; [2]Department of Medical Genetics, Osaka Medical Center and Research Institute for Maternal and Child Health, Izumi, Osaka, Japan; [3]Clinical and Molecular Genetics Unit, Institute of Child Health, Great Ormond Street Hospital for Children, University College London, London, UK; [4]Department of Pediatrics, Academic Medical Center, University of Amsterdam, Amsterdam, The Netherlands; [5]Department of Pediatric Oncology, Emma Children's Hospital, Academic Medical Center, Amsterdam, The Netherlands; [6]Division of Medical Genetics, Saitama Children's Medical Center, Saitama, Japan; [7]Department of Pediatrics, Central Hospital, Aichi Human Service Center, Aichi, Japan; [8]Department of Pediatrics and Child Health, Kurume University School of Medicine, Kurume, Japan; [9]Department of Pediatrics, Sapporo Medical University, Sapporo, Japan; [10]Division of Pediatrics, Oida Hospital, Kochi, Japan; [11]Department of Pediatrics, Hitachi Ltd, Mito General Hospital, Ibaraki, Japan; [12]Division of Medical Genetics, Kanagawa Children's Medical Center, Yokohama, Japan; [13]Department of Genetic Counseling, Ochanomizu University, Tokyo, Japan; [14]Department of Dermatology, Shinshu University School of Medicine, Matsumoto, Japan; [15]Department of Hematology and Oncology, Miyagi Children's Hospital, Sendai, Japan and [16]Department of Pediatrics, Tohoku University School of Medicine, Sendai, Japan
Correspondence: Dr Y Aoki, Department of Medical Genetics, Tohoku University School of Medicine, 1-1 Seiryo-machi, Sendai, Miyagi 980-8574, Japan.
E-mail: aokiy@med.tohoku.ac.jp
Received 14 June 2010; accepted 15 August 2010; published online 30 September 2010

identified in 60–80% of Noonan syndrome patients.[7–12] In patients with Costello syndrome, germline mutations in *HRAS* have been identified,[13] and mutations in *KRAS*, *BRAF* or *MAP2K1/MAP2K2* have been identified in approximately 70% of patients with CFC syndrome.[14,15] However, in approximately 40% of patients with these disorders, specific mutations have not been identified.

SHOC2 is homologous to *soc2*, a gene that was discovered in *Caenorhabditis elegans*. The *soc2* gene encodes leucine-rich repeats[16] and acts as a positive modulator of the RAS/MAPK pathway.[17] Recently, Cordeddu *et al.*[18] reported a gain-of-function missense mutation, c.4A>G (p.S2G), in *SHOC2* in patients with Noonan-like syndrome with loose anagen hair. However, clinical features of patients with a mutation in *SHOC2* remain unknown. In this study, we analyzed 92 patients with Noonan syndrome and related disorders to characterize mutations in the *SHOC2* gene. We also performed expression analysis of *SHOC2* in adult and fetal human tissues and performed sequence analysis of *SHOC2* in 82 leukemia samples.

MATERIALS AND METHODS

DNA samples from patients with Noonan syndrome and related disorders and from leukemia cells

We analyzed 92 patients with Noonan syndrome and related disorders who did not display *PTPN11*, *KRAS*, *HRAS*, *BRAF*, *MAP2K1/2* (*MEK1/2*), *SOS1* or *RAF1* mutations. At the time at which samples were sent, the primary diagnoses of these patients were as follows: 34 Noonan syndrome, 17 Costello syndrome, 21 CFC syndrome, 4 Noonan/CFC, 2 Costello/CFC and 14 others. Control DNA was obtained from 132 healthy Japanese individuals. Control DNA from 105 healthy Caucasian individuals was purchased from Coriell Cell Repositories (Camden, NJ, USA). Eighty-two leukemia DNA samples were collected from leukemia patients (32 acute myeloid leukemia, 41 acute lymphoblastic leukemia, 1 juvenile chronic myelogenous leukemia, 1 Ki-lymphoma, 2 malignant lymphoma, 1 myelodysplastic syndrome, 1 aplastic anemia, 2 transient abnormal myelopoiesis and 1 unknown). Nine additional genomic DNA samples were collected from patients who had developed leukemia and had achieved complete remission (eight acute lymphoblastic leukemia and one aplastic anemia).

This study was approved by the Ethics Committee of Tohoku University School of Medicine. We obtained informed consent from all subjects involved in the study and specific consent for photographs from seven patients.

Analysis of *SHOC2* mutations

Genomic DNA was extracted from patients' peripheral leukocytes. Exons and flanking intron sequences of *SHOC2* were amplified by PCR with primers based on GenBank sequences (Supplementary Table 1, GenBank accession no. NC_000010.10). The M13 reverse or forward sequence was added to the 5′ end of the PCR primers for use as a sequencing primer. PCR was performed in 15 μl of solution containing 67 mM Tris-HCl (pH 8.8), 6.7 mM $MgCl_2$, 17 mM NH_4SO_4, 6.7 μM EDTA, 10 mM β-mercaptoethanol, 1.5 mM dNTPs, 10% (v/v) dimethylsulfoxide (except fragment 7), 1 μM of each primer, 50 ng genomic DNA and 1 unit of Taq DNA polymerase. The reaction consisted of 37 cycles of denaturation at 94 °C for 20 s, annealing at the indicated temperature for 30 s and extension at 72 °C for 30 s. The PCR products of fragment 1a were gel purified; PCR products of the other fragments were purified using MultiScreen PCR plates (Millipore, Billerica, MA, USA). The purified PCR products were sequenced on an ABI PRISM 3130 automated DNA sequencer (Applied Biosystems, Foster City, CA, USA).

Development of a mutation detection system using the light cycler

Real-time PCR and melting curve analysis to detect the c.4A>G mutation was developed using the LightCycler system (Roche Diagnostics, Mannheim,

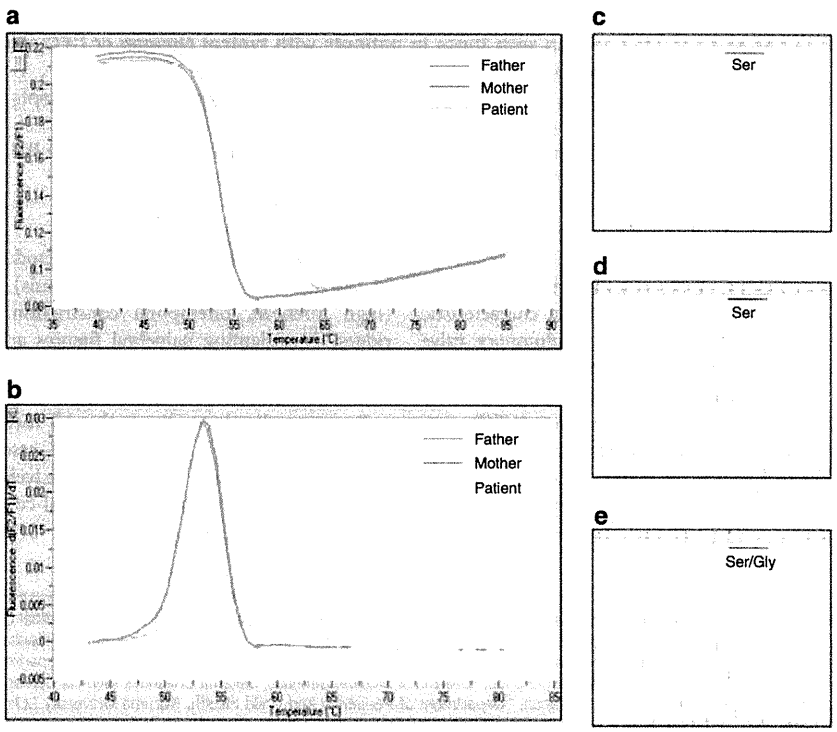

Figure 1 (**a**) PCR followed by melting analysis to detect the c.4A>G mutation. F2 represents the fluorescence emission of the LC Red 640 fluorophore, whereas F1 shows the fluorescence emission of the fluorescein fluorophore. (**b**) Melting curves are automatically converted into melting peaks, which are given as the first negative derivative of the fluorescence (F) versus temperature (T) (-dF/dT) (*y* axis) versus temperature (temp)(*x* axis). The homozygous wild-type allele (parents of NS128) shows a single melting temperature, whereas the heterozygote (NS128) shows two different melting temperatures. (**c**, **d**) Sequencing traces of parents of NS128. (**e**) Sequencing trace of NS128.

Germany). Primer and probe sequences are shown in Supplementary Table 2. The acceptor probe, which matches the mutant allele sequence, was labeled at its 3′ end with fluorescein isothiocyanate. The donor probe was labeled at its 5′ end with LC Red640 and phosphorylated at its 3′ end to prevent probe elongation by the Taq polymerase. Probes were designed by Nihon Gene Research Laboratories (Sendai, Japan). Amplification was performed in a final volume of 20 μl in glass capillaries containing 10 ng of sample DNA, 2 μl of 10× LightCycler-FastStart DNA Master HybProbe (Roche Diagnostics), 12 nM $MgCl_2$, 0.3 μM of each forward and reverse primer and 0.2 μM of each acceptor and donor hybridization probe. PCR was performed under the following conditions: initial denaturation at 95 °C for 10 min, 40 cycles of 95 °C for 10 s, 60 °C for 15 s and 72 °C for 7 s with a ramping time of 20 °C s^{-1}. After amplification, melting curve analysis was performed under the following conditions: 95 °C with 0-s hold, cooling to 40 °C for 30 s and slowly heating the sample to 85 °C with a ramp rate of 0.4 °C s^{-1}.

Real-time quantitative PCR

MTC Multiple Tissue cDNA panels Human 1, 2, Human Fetal, Human Immune and Human Cell Line (Clontech, Palo Alto, CA, USA) were used to evaluate the relative expression of *SHOC2* in various tissues. Separation of mononuclear and polymorphonuclear (PMN) leukocytes from whole blood was performed using Polymorphoprep (Nycomed, Oslo, Norway); total RNA was prepared with the RNeasy Mini Kit (Qiagen, Hilden, Germany). One hundred ng of total RNA was used to synthesize complementary DNA (cDNA) using the High Capacity cDNA Reverse Transcription kit (ABI). Primers for real-time PCR were designed using software provided by Roche (https://www.roche-applied-science.com) (Supplementary Table 3). Universal ProbeLibrary #42 and #60 (Roche) were used for *SHOC2* and *GAPDH*, respectively. PCR was performed in 20 μl of solution containing 10 μl FastStart Universal Probe Master (Rox) (Roche), 18 pmol of each primer, 5 μl cDNA and 0.25 μM universal HybProbe. The reaction conditions were 50 °C for 2 min and 95 °C for 10 min, followed by 40 cycles of 95 °C for 15 s and 60 °C for 11 min. The real-time PCR program was run by the 7500 Real-Time PCR system (ABI). Diluted control cDNA (1:1, 1:10, 1:100, 1:1000 and 1:10 000) from Multiple Tissue cDNA panels (Clontech) was amplified with each reaction in order to generate a standard curve and calculate relative gene expression of *SHOC2*.

RESULTS

Mutation analysis in patients and development of a rapid mutation detection system

Sequence analysis of all coding regions of *SHOC2* in 92 patients revealed a c.4A>G mutation (p.S2G) in exon1 of *SHOC2* in eight unrelated patients. Parental samples were available in three families; the mutation was not identified in parents, suggesting that the mutation occurred *de novo*.

Our results and the previous report identified a c.4A>G mutation in patients with Noonan-like syndrome. To further characterize the occurrence of this mutation, we developed a rapid mutation detection system using a Lightcycler. Two probes were generated for melting curve analysis, and melting curve analysis was performed after PCR. The PCR products from a patient heterozygous for the c.4A>G mutation differed from those obtained from the patient's parents as well as from those obtained from control subjects (Figures 1a and b). The PCR products were verified by sequencing (Figures 1c–e).

Clinical manifestations of patients with the *SHOC2* mutation

The clinical manifestations of eight patients with the *SHOC2* mutation are shown in Table 1; photographs of five of these patients are shown in Figure 2. The ages of the patients ranged from 4 to 25 years. The primary diagnoses for these patients were Costello, Noonan or CFC syndrome. Three had perinatal abnormalities, including tachypnea, hydramnios, pulmonary hemorrhage and intracranial hemorrhage.

Table 1 Clinical manifestations in *SHOC2* mutation-positive patients

Patient ID	*NS34*	*NS93*	*NS97*	*NS121*	*NS128*	*NS180*	*NS220*	*NS232*
SHOC2 mutation	p.S2G	p.S2G	p.S2G	p.S2G	p.S2G	p.S2G	p.S2G	p.S2G
Genotype of father/mother	WT/WT	ND	ND	ND	WT/WT	ND	ND	WT/WT
Gender	M	F	F	M	F	M	F	M
Age (years)	13.8	21	10	5.7	8	9	4	25
Country	Japan	The Netherlands	Japan	Japan	Japan	Japan	Japan	Japan
Primary diagnosis	NS/CFC	CFC	CFC	CFC	CFC	NS	CS	CS
Perinatal abnormality	+	ND	–	–	–	+	+	–
Polyhydramnios	–	ND	–	–	–	+	–	–
Birth weight	3118 g	3360 g	3068 g	2865 g	2308 g	3258 g	3160 g	3090 g
Others	Tachypnea					Pulmonary hemorrhage	Intracranial hemorrhage	
Growth and development								
Failure to thrive	+	+	+	+	+	+	+	+
Mental retardation	+ WISC III at 9 years 3 months VIQ 81, PIQ 87, FIQ 82	–	+ (DQ44)	+ (DQ48)	+ (DQ 66)	+ WISC III at 9 years 4 months VIQ 61, PIQ <40 FIQ 45	+ (DQ53)	+ (IQ65)
Hyperactivity	–	–	+	–	–	–	–	– (irritability in infancy)
Delayed independent walking (age)	+ (3.6 years)	–	+ (1.8 years)	+ (2.8 years)	+ (4 years)	+ (5 years)	+ (4 years)	+ (3.6 years)
Craniofacial characteristics								
Relative macrocephaly	+	+	+	+	+	+	+	+
Hypertelorism	+	–	–	–	–	+	–	+

Table 1 Continued

Patient ID	*NS34*	*NS93*	*NS97*	*NS121*	*NS128*	*NS180*	*NS220*	*NS232*
Downslanting palpebral fissures	+	+	+	–	–	+	–	–
Ptosis	–	+	–	+	–	–	–	–
Epicanthal folds	–	–	+	+	–	+	+	±
Low-set ears	+	+	+	+	+	+	+	+
Highly arched palate	+	+	–	+	+	–	+	+
Prominent forehead	ND	–	+	+	ND	ND	+	ND
Broad forehead	+	+	+	+	+	+	+	ND
Skeletal characteristics								
Short stature	−3.4 s.d. at 13 years	−3 s.d. at 21 years	−4 s.d. at 6 years	−3 s.d. at 1 year 9 months	−5 s.d. at 8 years	−6 s.d. at 9 years	−4.5 s.d. at 3 years 3 months	−2 s.d. at 23 years
Short neck	+	+	–	+	+	+	–	+
Webbing of neck	+	+	–	–	–	–	–	±
Cubitus valgus	+	+	–	–	–	–	–	–
Pectus anomalies	ND	–	+	+	–	+	–	–
Cardiac defects								
Hypertrophic cardiomyopathy	–	–	+	–	+	+	±	–
Atrial septal defect	–	–	+	–	–	–	+	+
Ventricular septal defect	–	–	–	–	–	–	–	+
Pulmonary stenosis	+	–	+	–	+	–	+	–
Mitral valve anomaly	+	–	–	–	–	–	–	+
Others	Pulmonary regurgitation	Arrhythmia						Hypoplasia of papillary muscle
Hair anomalies								
Curly hair	–	–	+	+	+	+	+	+
Sparse hair	+	+	+	+	+	+	+	+
Easily pluckable hair	+	+	+	+	+	ND	+	+
Skin anomalies								
Dark skin	+	+	+	+	+	+	+	+
Hyperkeratosis	ND	+	+	+	+	–	–	+
Hyperelastic skin	+	–	+	+	+	–	–	+
Café-au-lait spots	+	–	–	–	–	–	–	–
Lentigines	+	–	–	–	–	+	–	–
Atopic skin/eczema	+	+	+	+	+	+	+	+
Others					Deep palmar/ planter creases			Facial erythema, nummular eczema
Genital abnormalities	+ (Cryptorchidism)	–	–	–	–	+(Cryptorchidism)	–	–
Blood test abnormality								
Coagulation defect (normal range)	+[a]	ND	–	+[b]	ND	+[c]	–	–
Number of white blood cells(/μl)	7200	8400	16 000	5300	10 900	9900	10 300	9900
(normal range for patient's age)	(5000–10 000)	(5000–10 000)	(4500–13 500)	(6000–15 000)	(4500–13 500)	(4500–13 500)	(6000–15 000)	(5000–10 000)
Polymorph nuclear cell (%)	60 (55)	ND	79 (55)	ND	50 (55)	72 (55)	53 (45)	77 (55)
(mean for each patient's age)								
IgE ($U ml^{-1}$)	ND	ND	2300	94	ND	1800	ND	820
Hypernasal/hoarse voice	ND	–	+	+	–	ND	+	+
Miscellaneous	GH deficiency	Delayed puberty, EEG abnormalities, easy bruising	GH deficiency	GH deficiency	Adenoid hypertrophy, GH deficiency		Dilatation of cerebral ventricles, epilepsy	Congenital hydro-nephrosis, frostbite in winter

Abbreviations: APTT, activated partial thrombin time; AT, antithorombin; BT, bleeding time; CFC, cardio-facio-cutaneous; CS, Costello syndrome; DQ, developmental quotient; EEG, electroencephalogram; FIQ, Full Scale intelligence quotient; GH, growth hormone; ND, not described; NS, Noonan syndrome; PIQ, Performance intelligence quotient; PT, prothrombin time; VIQ, verbal intelligence quotient; WISC, Wechsler Intelligence Scale for Children; WT, wild type.
[a]The test was performed when bloody stool was observed at 7 years of age. BT 180 sec (2.5–13), PT 11.5 sec (10.1–12.0) APTT 62.5 sec (26–37), Factor VIII 53% (52–120). Parenthesis represents normal range for the patient's age.
[b]APTT 54 sec (26–37), Factor IX 22% (47–104), Factor XII 34% (64–129), Factor XIII 51 (72–143). Parenthesis represents normal range for the patient's age.
[c]APTT 57 sec (26–37). Parenthesis represents normal range for the patient's age.

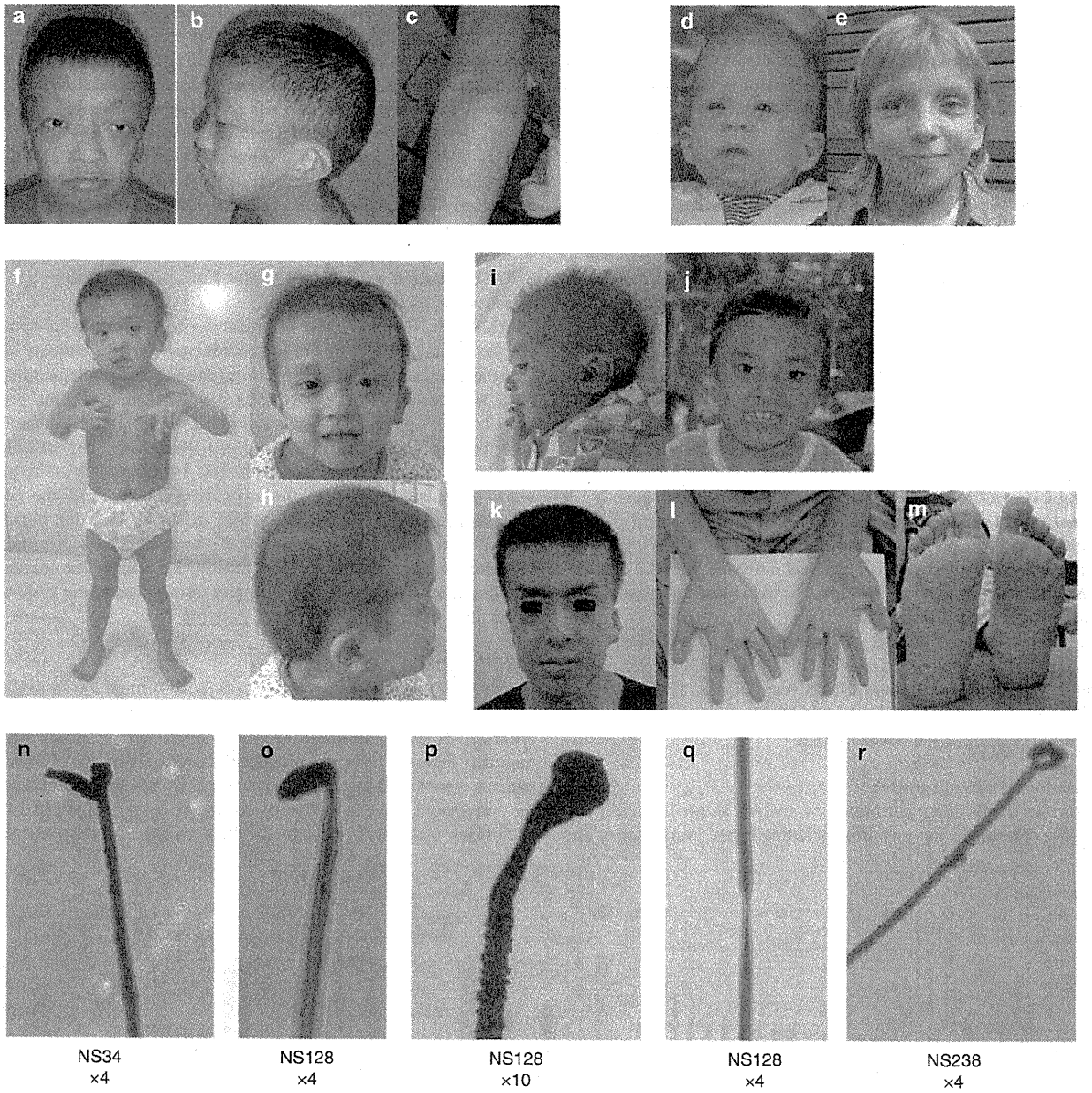

Figure 2 (**a**, **b**) Facial appearance of NS34 at the age of 13 years. (**c**) Dry and atopic skin seen in NS34. (**d**, **e**) NS93. (**f–h**) NS97. (**i**, **j**) NS128. (**k–m**) NS232 at the age of 25 years. (**l**, **m**) Palms and soles of NS232 showing fine wrinkling. Light micrographs of hairs from patients NS34 (**n**), NS128 (**o–q**) and NS238 (**r**). The hair bulb is distorted at an acute angle to the hair shaft, a characteristic described as 'mousetail deformity.' The hair shaft is twisted and longitudinally grooved.

All showed short stature $\geqslant -2$ s.d.) despite normal growth during the fetal period. Mild-to-moderate mental retardation was observed in seven patients. It is of note that delayed independent walking was observed in seven patients. The facial appearances of these patients changed with age. Features frequently observed were relative macrocephaly (8/8 patients), low-set ears (8/8), highly arched palate (6/8) and broad forehead (7/7). Cardiac abnormalities included hypertrophic cardiomyopathy in four patients, atrial septal defect in three patients, pulmonic stenosis in four patients and mitral valve anomaly in two patients. Atopic skin and eczema were observed in all eight patients (Figure 2c), and serum immunoglobulin E level was elevated in three patients. Seven patients had sparse and easily pluckable hair. The hair bulb was bent at an acute angle to the hair shaft, which was irregular and twisted (Figures 2n–r). Four patients had hyponasal/hoarse voice as previously described[18] and three patients showed coagulation defects with prolonged activated partial thrombin time.

The clinical history of two adult patients, NS232 and NS93, differed from those of patients typical for Noonan syndrome. NS232 was a 25-year-old patient, the first son of unrelated healthy parents. Delivery

at 40 weeks was uncomplicated, and birth weight was 3090 g. At 1 month of age, this patient was diagnosed as having an atrioventricular septal defect; the defect spontaneously closed at 5 months of age. During the infantile period, this patient showed irritability and mental/motor delay: head control was achieved at 1 year and 10 months, sitting at 2 years and 4 months and walking at 3 years and 6 months. At his infantile period, this patient was suspected to have Noonan syndrome or Costello syndrome. Pyelostomy for congenital hydronephrosis was performed at the age of 10 months. At 23 years of age, mitral valve replacement was performed because of mitral valve prolapse (III–IV). The dissected mitral valve showed myxomatous change. At 25 years, this patient shows mild mental retardation and displays a gentle personality. Other characteristics include hypertelorism, a highly arched palate and posteriorly rotated ears. During infancy, his hair was pluckable, but the hair abnormality is now subtle. He possesses variable skin abnormalities including fine wrinkles on the palm and soles as well as erythematous rash on the face and eczematous skin changes on the trunks and extremities together with xerotic skin, which are reminiscent of atopic dermatitis (Figures 2k–m). Another adult patient, NS93, has been diagnosed as having CFC syndrome at 1 year of age (Figure 2d). Subsequently her normal motor development and her cognitive development that fell within normal ranges (but was lower than other family members) shed doubt about this diagnosis. She had a delayed pubertal development. She has quite a marked tendency to have bleeding episodes after surgery and to bruise easily.

Leukocytosis in the absence of obvious infection was observed in one of the patients (NS97). The white blood cell count of this patient ranged from 16 000 to 23 000/μl at 5 years of age. The number of leukocytes of the other patients was within the normal range, but close to the upper limit of the normal range.

Expression of *SHOC2* mRNA

A previous study using northern blot analysis showed that *SHOC2* mRNA is present in most tissues, including brain, heart, kidney and pancreas.[16] Because leukocytosis was observed in a patient with the p.S2G mutation, we examined the relative expression of *SHOC2* in various tissues including blood leukocytes and lymphocytes. In the adult human cDNA panel, the highest expression was observed in testis; relatively high expression was also observed in several immune tissues (spleen, bone marrow, tonsil and lymph node) (Figures 3a and b). The expression of *SHOC2* was six times higher in PMN than mononuclear (Figure 3c). Among fetal tissues, brain showed the highest expression (Figure 3d). No increase in *SHOC2* expression was observed in cultured tumor cells (Figure 3e).

SHOC2 mutation analysis in samples from patients with hematologic malignancies

Patients with Noonan-related disorders develop various solid tumors and hematologic malignancies.[5] Approximately 10% of patients with Costello syndrome develop rhabdomyosarcoma, ganglioneuroblastoma or bladder carcinoma. Patients with Noonan syndrome occasionally develop juvenile myelomonocytic leukemia or leukemia.[2] Recently, the occurrence of ALL or non-Hodgkin's lymphoma has been reported in three patients with CFC syndrome.[5,19,20] The presence of leukocytosis in mutation-positive patients and the high expression of *SHOC2* mRNA in PMN led us to look for possible *SHOC2* mutations in patients with hematologic malignancies. However, no such mutations were identified in any of the leukemia samples or in the genomic DNA samples from patients who had been treated for leukemia.

DISCUSSION

In this study, we identified the c.4A>G (p.S2G) mutation in *SHOC2* in 8 of 92 (9%) otherwise mutation-negative patients with Noonan syndrome or related disorders. The mutation detection rate was higher than that reported in a previous study, in which 21 of 410 (5%) such patients were found to carry this mutation. By parental examination, the current and previous studies confirmed *de novo* mutation in 3 and 12 families, respectively. Quantitative PCR analysis demonstrated that

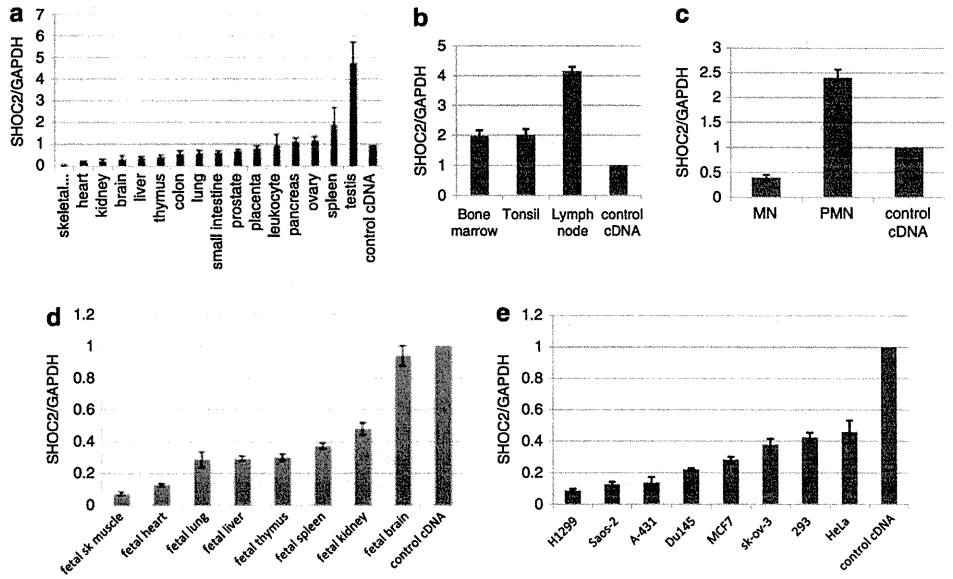

Figure 3 Relative expression of *SHOC2*. Expression levels of *SHOC2* mRNA in various adult human tissues (**a**), adult immune tissues (**b**), human leukocytes (**c**), human fetal tissues (**d**) and human tumor cell lines (**e**) were evaluated by quantitative PCR using *GAPDH* mRNA as the control. Results are expressed as the means and s.d.s of mean values from triplicate samples. Control DNA supplied with Clontech cDNA panels was used as a control.

Table 2 Summary of clinical manifestations in patients with CFC syndrome, Noonan-like syndrome and Noonan syndrome

	CFC syndrome (%)	*Noonan-like syndrome (%)*	*Noonan syndrome (%)*
References	20,21[a]	Cordeddu *et al.*[18] and this study	22
Gene mutations	*KRAS*, *BRAF* and *MAP2K1/2*	*SHOC2*	*PTPN11*, *KRAS*, *SOS1* and *RAF1*
Total patients	63	33	315
Perinatal abnormality			
Polyhydramnios	23/30 (77)	1/7 (14)	21/50 (42)
Fetal macrosomia	ND	ND	20/46 (43)
Growth and development			
Failure to thrive	24/36 (67)	8/8 (100)	51/74 (69)
Mental retardation	25/25 (100)	27/32 (84)	124/293 (42)
Craniofacial characteristics			
Relative macrocephaly	40/58 (69)	31/33 (94)	50/70 (71)
Hypertelorism	17/25 (68)	26/33 (79)	66/82 (80)
Downslanting palpebral fissures fissures fissures	20/25 (80)	4/8 (50)	77/99 (78)
Ptosis	12/25 (48)	24/33 (73)	75/105 (71)
Epicanthal folds	13/25 (52)	5/8 (63)	41/72 (57)
Low-set ears	20/25 (80)	30/33 (91)	115/132 (87)
Skeletal characteristics			
Short stature	46/63 (73)[b]	32/32 (100)	172/297 (58)
Short neck	22/25 (88)	23/33(70)	76/107 (71)
Webbing of neck	6/25(24)	20/33 (61)	84/188 (45)
Cardiac defects			
Hypertrophic cardiomyopathy	24/58 (41)	9/33 (27)	57/277 (21)
Atrial septal defect	11/57 (19)	11/33 (33)	20/69 (29)
Ventricular septal defect	7/57 (12)	3/33(9)	7/70 (10)
Septal defect total	18/57 (32)	14/33 (42)	85/313 (27)
Pulmonic stenosis	23/58 (40)	13/33 (39)	196/312 (63)
Patent ductus arteriosus	ND	0/33 (0)	3/38 (8)
Mitral valve anomaly	10/63 (16)[a]	10/32 (31)	16/67 (24)
Arrhythmia	4/63 (6)	1/33 (3)	14/25 (56)
Skeletal/extremity deformity			
Cubitus valgus	6/25 (24)[a]	2/8 (25)	26/100 (26)
Pectus deformity	27/54 (50)	23/32 (72)	184/287 (64)
Skin/hair anomaly			
Curly hair	58/63 (92)	6/8 (75)	30/75 (40)
Sparse hair	56/63 (89)	33/33 (100)	ND
Loose anagen hair/easily pluckable hair	ND	19/19(100)	ND
Hyperelastic skin	7/25 (28)[a]	5/8 (63)	16/51 (31)
Café-au-lait spots	13/58 (22)[a]	1/8 (13)	5/49 (10)
Lentigines	ND	2/8 (25)	3/49 (6)
Nevus	37/62 (60)[a]	ND	12/46 (26)
Genitalia			
Cryptorchidism	11/41(27)[a]	8/25 (32)	114/211 (54)
Blood test abnormality			
Coagulation defects	1[c]	9/29 (31)	65/180 (36)

Abbreviations: CFC, cardio-facio-cutaneous; ND, not described.
[a]Includes our unpublished data.
[b]Includes short stature (height below the 3rd centile).
[c]A patient with von Willebrand disease was reported.